Electronic Supplementary Material (ESI) for Materials Chemistry Frontiers.

Supporting Information

for

Theoretical Insights into Rational Design of Small Organic Phototheranostic Agents for Promoted Image-Guided Cancer Surgery

Jia Zhang,[a] Junfang Yang,[b] Yi Zeng,[a] Ze-Sheng Li,[a] Xiaoyan Zheng*[a,c]

[a] Key Laboratory of Cluster Science of Ministry of Education, Key Laboratory of Medicinal Molecule Science and Pharmaceutics Engineering of Ministry of Industry and Information Technology, Beijing Key Laboratory of Photoelectronic/Electrophotonic Conversion Materials, School of Chemistry and Chemical Engineering, Beijing Institute of Technology, 100081 Beijing, P. R. China.

[b] School of Chemical Sciences, University of Chinese Academy of Sciences, Beijing, 100049, P. R. China

[c] Guangdong Provincial Key Laboratory of Luminescence from Molecular Aggregates (South China University of Technology), Guangzhou 510640, China

Email: xiaoyanzheng@bit.edu.cn

Contents

Computational details…….....….....….....S3

Scheme S1 Chemical structure of TI and TSSI.....….....S6

Figure S1 Representative models for TSSI…….....….....….....S7

Figure S2. The extracted conformation of single molecule in dilute solution of TI and TSSI.....S8

Figure S3. The electron density contours of LUMO, HOMO and HOMO-1 of TI and TSSI at S_1..S9

Scheme S2 Chemical structure of TSSSSI.....….....….....S10

Figure S4 Optimized S_0 and S_1 geometries for designed four molecules.….....….....S11

Figure S5 The LUMO, HOMO and HOMO-1 in S_1 geometry for designed molecules…….....S12

Figure S6 The *t* index of TSSI and designed molecules.....….....S13

Figure S7 Optimized S_0 and S_1 geometries of (a) TI in monomer and (b) TSSI in monomer and aggregates.....S14

Figure S8 The HOMO and LUMO in S_1 geometry for TSSI in aggregates…….....…..S15

Figure S9 The orbital delocalization index for TSSI in monomer and aggregates.…….…….....S16

Figure S10 The energy levels and ΔE_g in S_1 state for TSSI in aggregates.……..….…….....…..S17

Figure S11 The absorption and emission spectrum for TSSI in aggregates.....….....S18

Table S1 Calculated the excitation energies using different functionals with 6-31G**.....….....S19

Table S2 The dihedral angles at the S_0 and S_1 for TI and TSSI in monomer……..S20

Table S3 The ΔE_{vert}, *f* and transition orbitals assignments of TI and TSSI in monomer.....S21

Table S4 The dihedral angles at the S_0 and S_1 for designed molecules……...….....S22

Table S5 The ΔE_{vert}, *f*, transition orbitals assignments, λ_{total} and k_r for designed molecules.….....….....S23

Table S6 The dihedral angles at the S_0 and S_1 for TSSI in aggregates.....….....S24

Table S7 The ΔE_{vert}, *f*, transition orbitals assignments, λ_{total}, k_r, k_{ic} and Φ_F for TSSI in aggregates.....S25

Supplementary Computational methods

For the TSSI in solution and the amorphous aggregates, different models were set up and calculate their photophysical properties, respectively (Fig. S1).

PCM model. The implicit polarizable continuum model (PCM)[1, 2] was chosen to simulate the dispersed monomer of both TI and TSSI by the Gaussian 16 software package[3] (Fig. S1a). A sequence of density functionals, including B3LYP,[4] ωB97XD,[5, 6] BMK[7] and M06-2X,[8] with the 6-31G** basis set,[9] were selected to calculate the excitation energies of the optimized structures in both the ground (S_0) and the first excited (S_1) states for TSSI in dilute solution and to find the most proper density functional, which could reproduce the experimental results (see Table S1). It is found that BMK combined with the 6-31G** basis set presents the best performance in reproducing the experimental results, the calculated maximum absorption and emission wavelengths (632 and 850 nm) are close to the experimental values (670 and 835 nm)[10] and was chosen to calculate the photophysical properties of all systems in this work. The optimized structures at S_0 and S_1 were obtained by DFT and TDDFT. In addition, normal mode analysis for all optimized structures were evaluated to check the absence of imaginary frequencies.

MD simulations. The atomic type and related force field parameters of TI and TSSI were generated by the general Amber force field (GAFF).[11] The restrained electrostatic potential approach was used to obtain the partial charge of each atom in TI and TSSI.[10] Based on the force field parameters, the molecular dynamics (MD) simulations of single TI and TSSI were also performed by putting one TI or TSSI into a cubic box with side length 7.0 nm and solvating by 11200 and 11194 water molecules, respectively. Then the energy minimization by the steepest descent algorithm were performed, followed by 100 ns production of MD simulations under NPT (T = 300 K and P = 1 bar) ensemble with a Berendsen thermostat and barostat.[12, 13] In addition, the aggregation process of TSSI in aqueous solution were also simulated by MD simulations. First, we randomly placed 60 TSSI molecules into a small cubic box with dimensions of 5 × 5 × 5 nm^3 to pre-assemble the amorphous aggregates. Second, the obtained amorphous aggregates of TSSI were put in the center of the cubic boxes with larger side lengths of 9 nm, and solvated by 22199 water molecules to obtain the initial conformation of the amorphous aggregates. Third, the energy minimization by the steepest descent algorithm and 100 ns production MD simulations under NPT ensemble were also performed with the Berendsen thermostat and Berendsen barostat. The time step for MD simulations of the TSSI aggregation process

was 2 fs. The configurations were stored at a time interval of 10 ps for data analysis. All MD simulations were performed using the GROMACS package (version 5.1.5).[14]

QM/MM calculations. Based on the obtained amorphous aggregates of TSSI, the QM/MM models were set up to study their photophysical properties. Due to loose and disorder molecular packing for TSSI, we randomly selected three amorphous aggregates at equilibrium from the MD simulations and set up QM/MM models, respectively. In the QM/MM model, one TSSI (completely enclosed in the aggregate) was chosen and set as the QM region, while the others were treated as the MM region (Fig. S1c). The QM region was calculated at the (TD)-BMK/6-31G** level and the MM region was treated by the universal force field.[15] All atoms in the QM region could be fully relaxed during the geometric optimization, while the others in the MM region were frozen. The electrostatic embedding scheme with QM polarization was adopted.[13] The normal mode frequency calculations for all the optimized structures at both S_0 and S_1 were performed to guarantee no imaginary frequencies for the optimized structures. All the QM/MM calculation were performed in Gaussian 16 package.[3]

Orbital delocalization index (ODI) and t index. The orbital delocalization index (ODI), which can quantitatively measure the degree of orbital delocalization, was calculated by using Multiwfn program.[16] The ODI of the *i*-th molecular orbital can be expressed as: $ODI_i = 0.01 \times \sum_A (\theta_{A,i})^2$. Herein, $(\theta_{A,i})^2$ is the composition of atom A in the *i*-th molecular orbital. The small ODI leads to large orbital delocalization. The t index quantitatively measure the degree of separation between the hole and the electron, was calculated by using Multiwfn program.[16]

Spin-orbital coupling constant (ξ). The spin-orbital coupling constant (ξ) affects the intersystem crossing process (ISC) and determine the ROS generation efficiency as well as photodynamic therapy efficiency. Since BMK not available in ORCA,[17] we adopted BHandHLYP with similar HF ratio combined with the 6-31G** basis set to calculate ξ.

Radiative decay rate (k_r). The radiative decay rate (k_r) was calculated according to the simple spontaneous emission relationship, $k_r = \frac{1}{1.499} f \Delta E_{vert}^{\ 2}$, where f is the oscillator strength, and ΔE_{vert} is the vertical excitation energy at the optimized S_1 geometry in units of cm^{-1}.

Reorganization energy (λ). The reorganization energy (λ) was calculated by TVCF protocol through MOMAP program.[18-20] And it reflects the geometrical changes between two electronic states and

affects nonradiative decay rate constant (k_{ic}). The reorganization energy can be expressed as a summation of the contributions from normal mode (NM) relaxation in the harmonic oscillator approximation:

$$\lambda = \lambda_{gs} + \lambda_{es} \tag{1}$$

$$\lambda_{gs} = \sum_{k \in gs} \lambda_k = \sum_{k \in gs} \hbar \omega_k HR_k \tag{2}$$

$$\lambda_{es} = \sum_{k \in es} \lambda_k = \sum_{k \in es} \hbar \omega_k HR_k \tag{3}$$

$$HR_k = \frac{\omega_k D_k^2}{2\hbar} \tag{4}$$

where HR_k represents the Huang−Rhys factor for the ^{k}th mode and D_k is the displacement for the mode k between the equilibrium geometries of S_0 and S_1.

Supplementary Figures

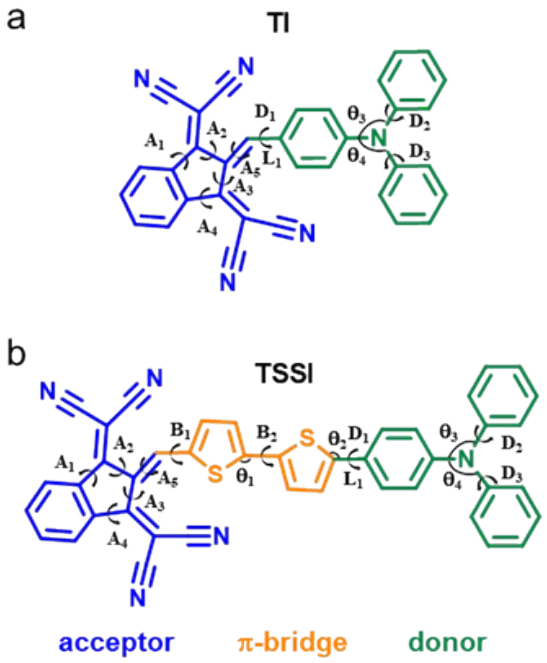

Scheme S1. Chemical structure of (a) TI and (b) TSSI. The acceptor, π-bridge, and donor are labeled in blue, orange and green, and the corresponding bond length (L_1), bond angles ($\theta_{n=1-4}$) and dihedral angles ($A_{n=1-5}$, $B_{n=1-2}$, and $D_{n=1-3}$), respectively.

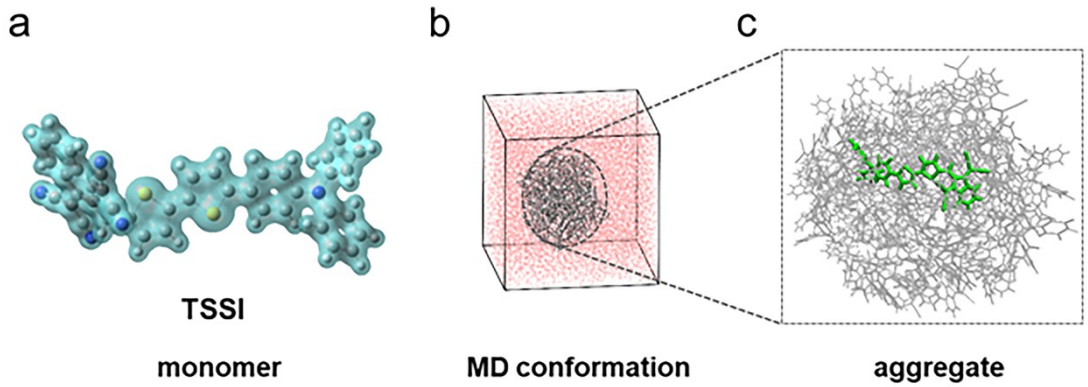

Figure S1. (a) The PCM model of TSSI in dilute chloroform solution. (b) The extracted configuration of TSSI in amorphous aggregate from the MD simulation and (c) the corresponding QM/MM model. Here one central TSSI was selected as the QM region, while the others as the MM region, respectively.

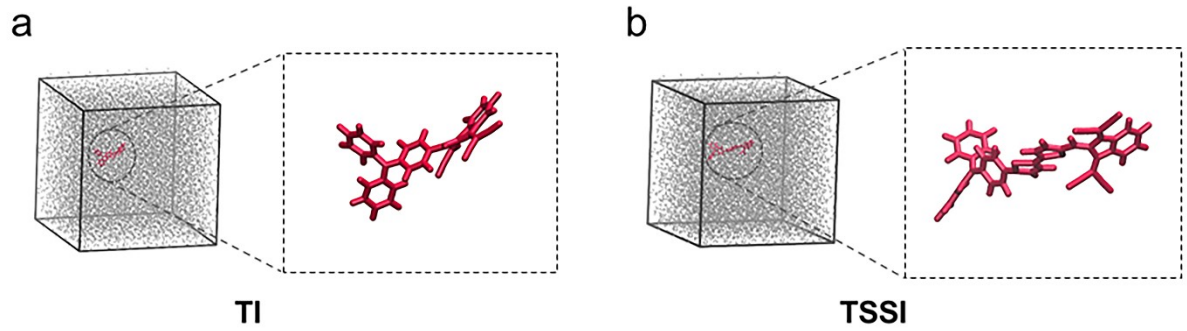

Figure S2. (a-b) The extracted representative conformation of single molecule in dilute solution of TI and TSSI.

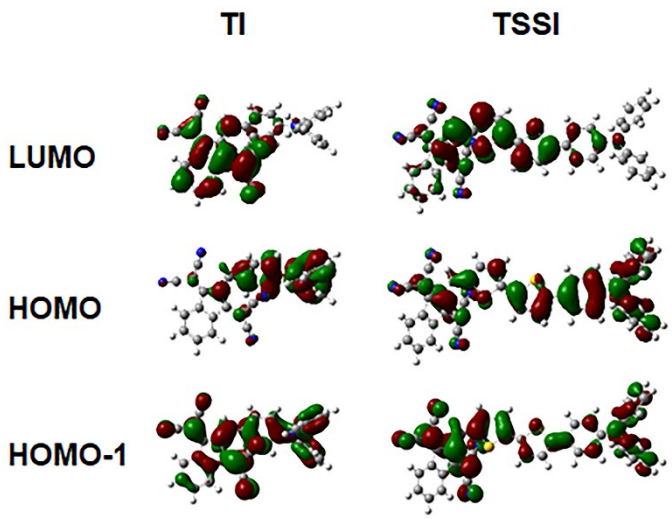

Figure S3. The electron density contours of LUMO, HOMO, and HOMO-1 for TI and TSSI in dilute chloroform solution at S_1 geometry.

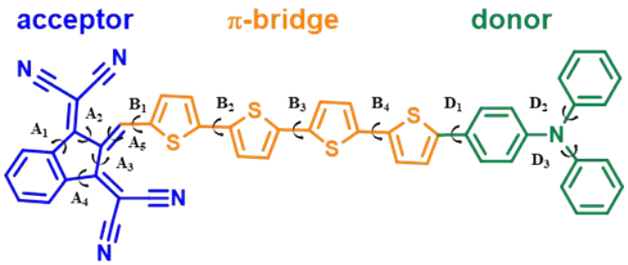

Scheme S2. Chemical structure of TSSSSI. The acceptor, π-bridge, and donor are labeled in blue, orange and green. The corresponding dihedral angles of TSSSSI are labeled in $A_{n=1-5}$, $B_{n=1-4}$ and $D_{n=1-3}$, respectively.

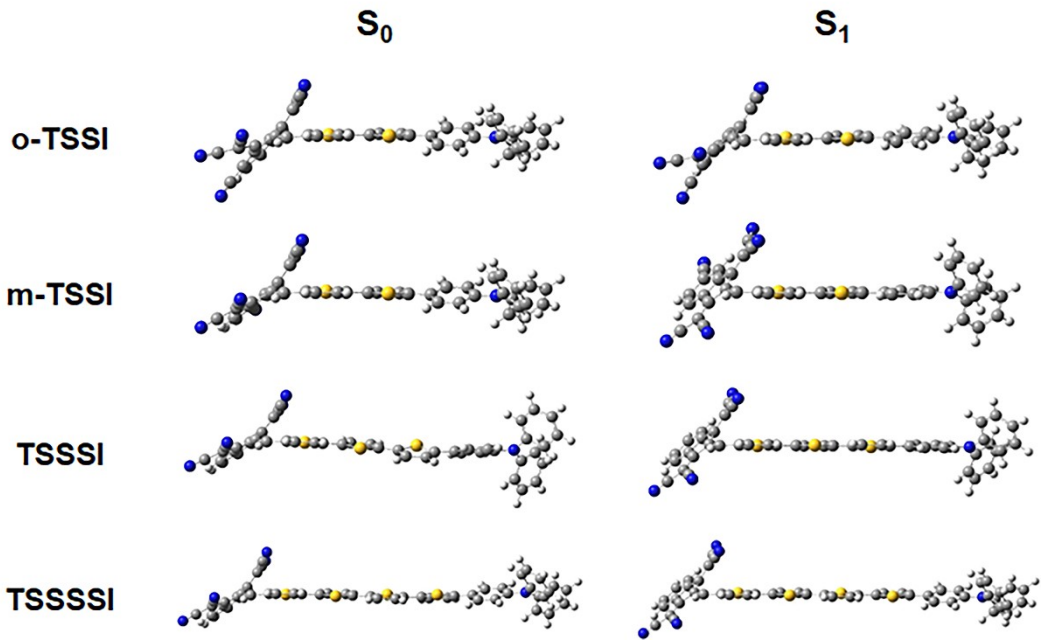

Figure S4. The optimized geometries of o-TSSI, m-TSSI, TSSSI and TSSSSI at both S_0 and S_1 in dilute chloroform solution at the BMK/6-31G** level.

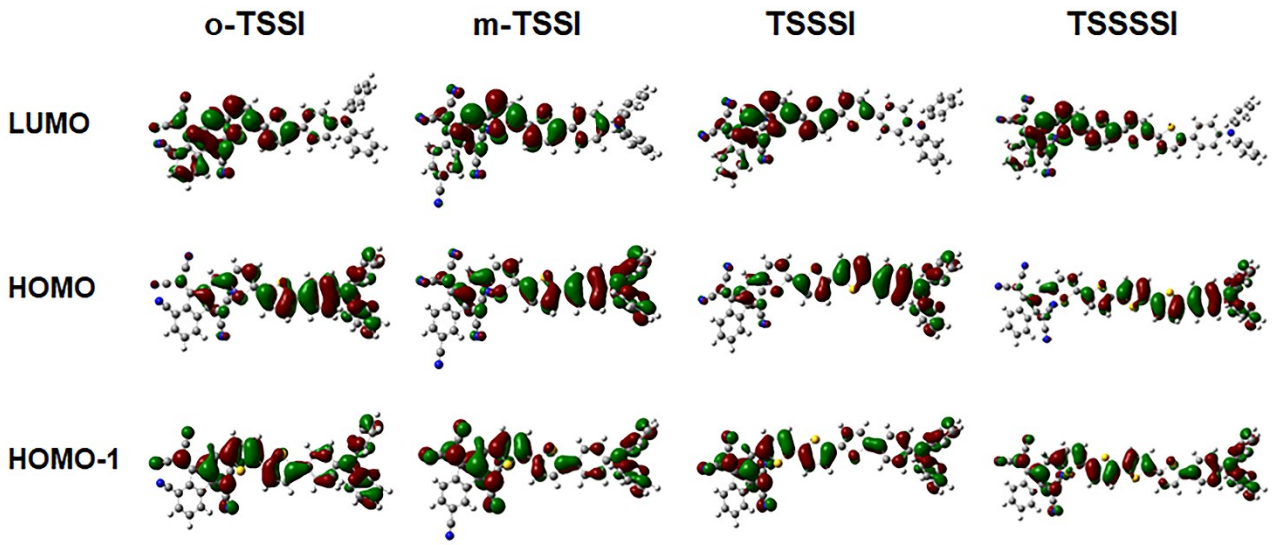

Figure S5. The electron density contours of LUMO, HOMO and HOMO-1 of o-TSSI, m-TSSI, TSSSI and TSSSSI in dilute chloroform solution at S_1 geometry.

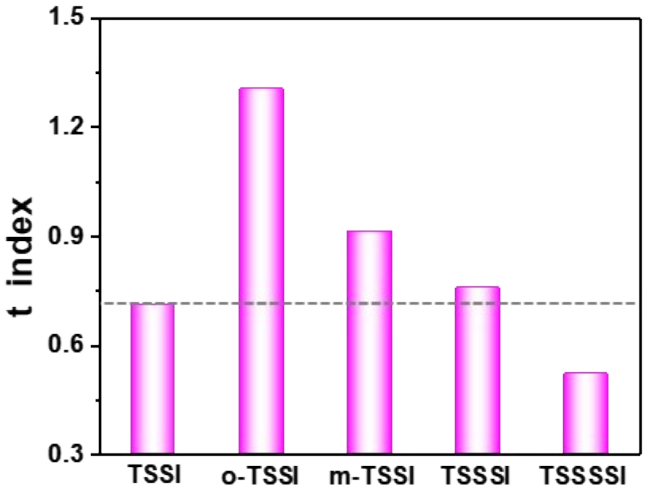

Figure S6. The *t* index of TSSI, o-TSSI, m-TSSI, TSSSI and TSSSSI at S_0 geometry.

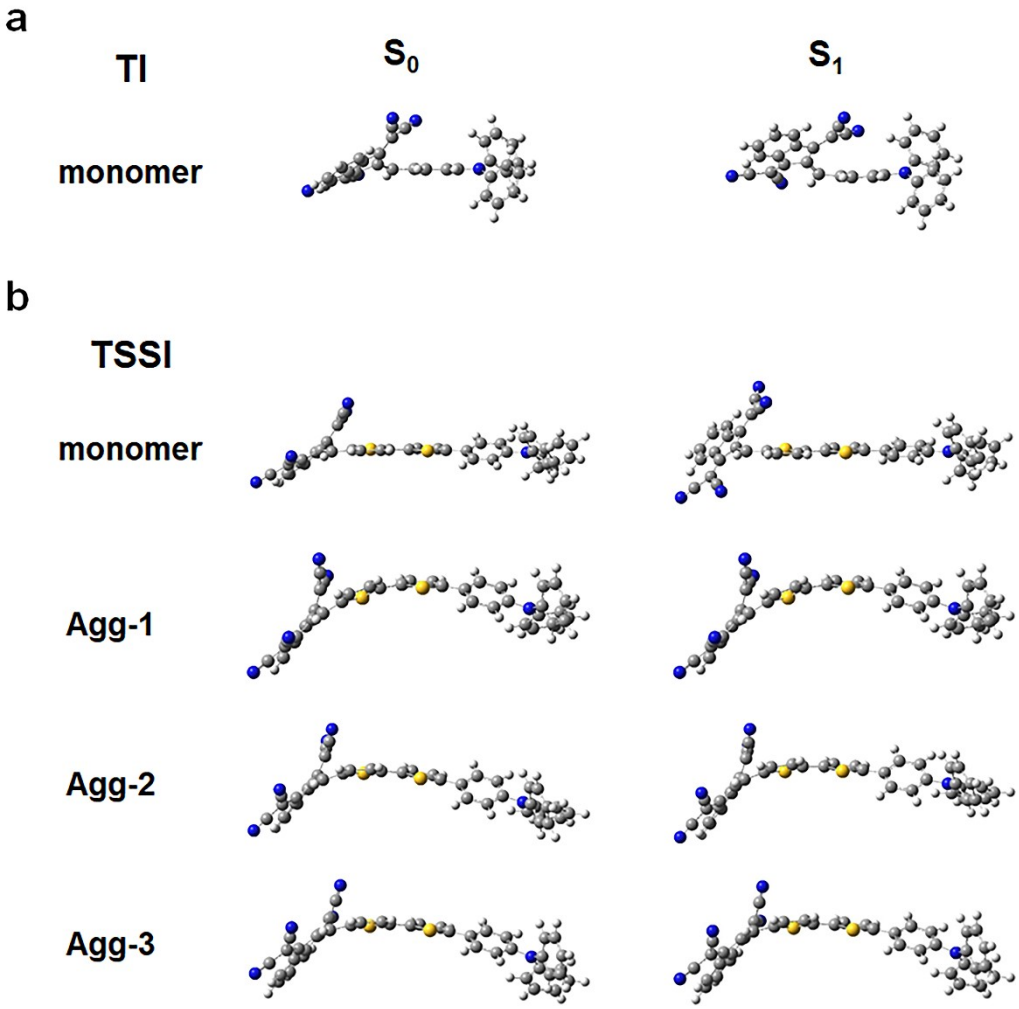

Figure S7. Optimized geometries at S_0 and S_1 of (a) TI in dilute chloroform solution and (b) TSSI in dilute chloroform solution and aggregated state. Agg-1, Agg-2 and Agg-3 are three representative aggregates extracted from MD trajectories.

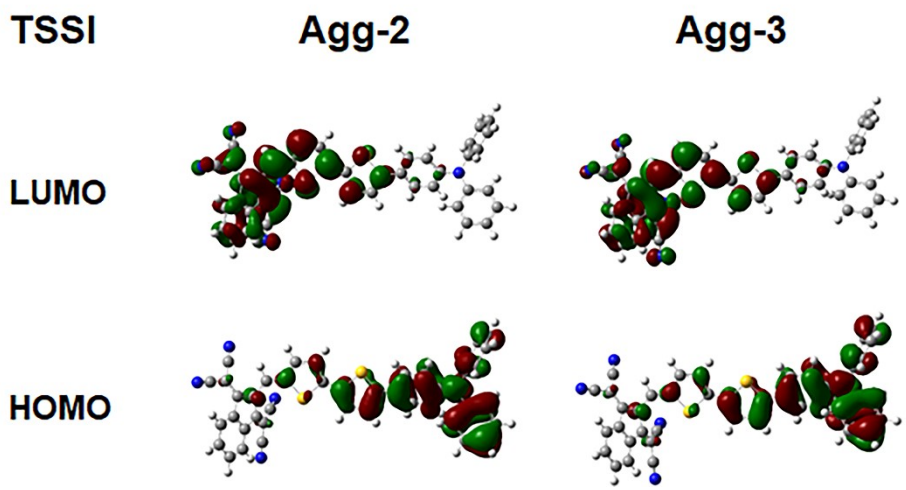

Figure S8. The electron density contours of LUMO and HOMO in S_1 geometry in aggregates for TSSI.

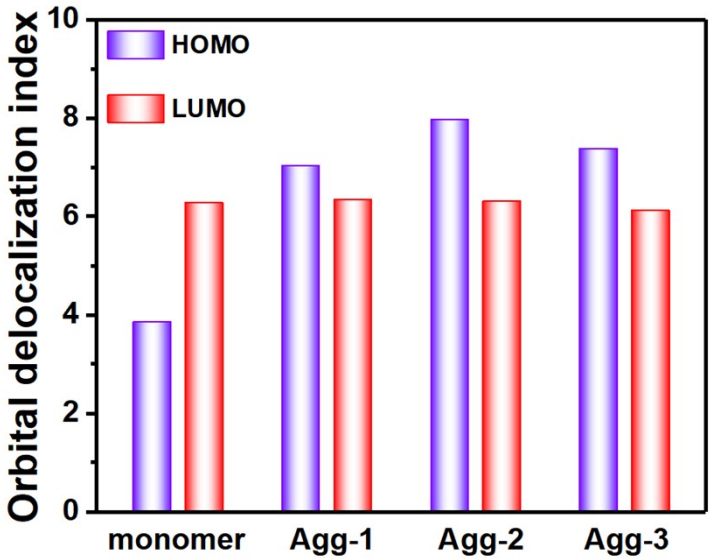

Figure S9. The orbital delocalization index of HOMO and LUMO for TSSI in dilute solution and aggregated state at S_1-geometry. Agg-1, Agg-2 and Agg-3 are three representative aggregates extracted from MD trajectories.

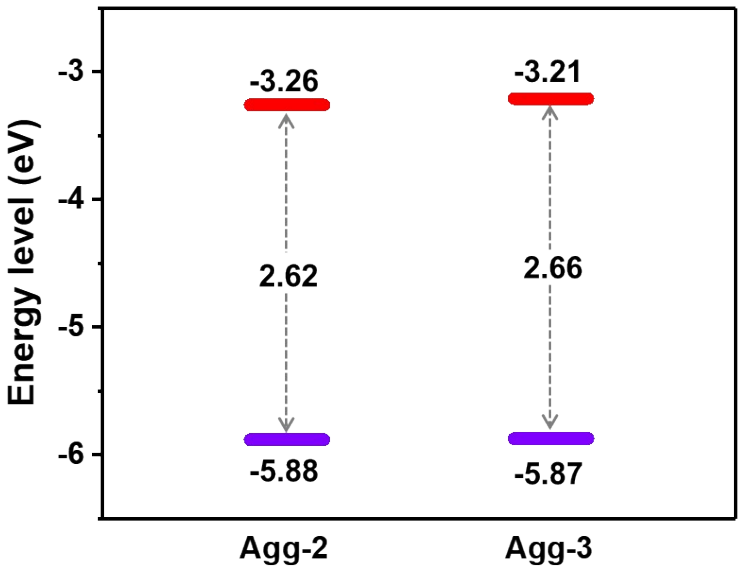

Figure S10. The energy levels and energy gaps (ΔE_g) of TSSI aggregates at S_1-geometry.

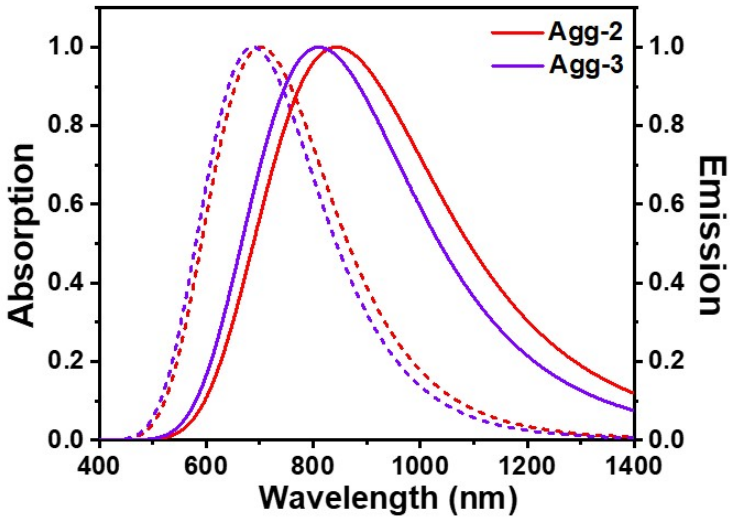

Figure S11. The absorption and emission spectrum of TSSI in aggregated states.

Supplementary Tables

Table S1. The calculated absorption and emission wavelength of TSSI in dilute chloroform solution by PCM model at several different density functionals with 6-31G** basis set, respectively.

	B3LYP	ωB97XD	BMK	M06-2X	Exper. [10]
Absorption	818 nm (1.52 eV)	498 nm (2.49 eV)	632 nm (1.96 eV)	552 nm (2.25 eV)	670 nm (1.85 eV)
Emission	969 nm (1.28 eV)	1636 nm (0.76 eV)	850 nm (1.46 eV)	1885 nm (0.66 eV)	835 nm (1.49 eV)

Table S2. The key bond length (Å), bond angles (degree) and dihedral angles (degree) for TI and TSSI in monomer at the S_0 and S_1 minimum.

	TI			**TSSI**		
	S_0	**S_1**	**$\|\Delta(S_0\text{-}S_1)\|$**	**S_0**	**S_1**	**$\|\Delta(S_0\text{-}S_1)\|$**
L_1	1.48	1.46	**0.02**	1.47	1.44	**0.03**
θ_1				120.7	121.4	**0.7**
θ_2				121.4	121.8	**0.4**
θ_3	119.2	120.0	**0.8**	120.7	121.1	**0.4**
θ_4	119.4	120.5	**1.1**	120.6	121.1	**0.5**
A_1	13.6	10.6	**3.0**	12.2	1.2	**13.4**
A_2	28.6	25.3	**3.3**	30.0	1.7	**28.3**
A_3	38.2	26.9	**11.3**	41.6	15.5	**26.1**
A_4	22.6	10.5	**12.1**	23.2	13.2	**10.0**
A_5	12.1	5.0	**7.1**	14.0	46.2	**32.2**
B_1				13.6	7.1	**6.5**
B_2				2.8	0.2	**2.6**
D_1	21.1	40.4	**19.3**	23.5	9.7	**13.8**
D_2	24.7	32.1	**7.4**	31.7	26.6	**5.1**
D_3	25.1	35.1	**10.0**	31.6	26.6	**5.0**

Table S3. Calculated vertical excitation energy (ΔE_{vert}) (eV), *f* and transition orbitals assignments of TI and TSSI in monomer.

	ΔE_{vert}	*f*	assignments
TI	1.71	0.1839	HOMO→LUMO (87.17%) HOMO-1→LUMO (8.10%)
TSSI	1.46	1.6279	HOMO→LUMO (84.78%) HOMO-1→LUMO (12.59%)

Table S4. Selected dihedral angles (degree) of designed molecules at the S_0 and S_1 minimum.

	o-TSSI			m-TSSI			TSSSI			TSSSSI		
	S_0	**S_1**	**$\|\Delta(S_0-S_1)\|$**	**S_0**	**S_1**	**$\|\Delta(S_0-S_1)\|$**	**S_0**	**S_1**	**$\|\Delta(S_0-S_1)\|$**	**S_0**	**S_1**	**$\|\Delta(S_0-S_1)\|$**
A_1	30.5	28.4	**2.1**	11.7	1.3	**13.0**	12.3	0.2	**12.5**	12.5	0.7	**11.7**
A_2	40.2	29.9	**10.3**	27.8	1.3	**26.5**	29.7	3.5	**26.2**	29.9	5.9	**24.0**
A_3	40.8	30.1	**10.7**	40.0	16.1	**24.0**	41.4	18.7	**22.7**	41.6	21.1	**20.4**
A_4	24.4	21.6	**2.8**	23.5	14.3	**9.2**	23.3	15.3	**8.0**	23.5	16.2	**7.3**
A_5	15.5	29.3	**13.8**	16.6	45.1	**28.4**	13.6	41.6	**28.0**	13.8	39.0	**25.3**
B_1	13.5	9.6	**3.9**	11.8	8.6	**3.2**	14.1	8.6	**5.5**	14.6	7.8	**6.9**
B_2	3.5	0.9	**2.6**	-0.7	0.7	**1.4**	8.4	0.4	**8.0**	6.1	1.6	**4.5**
B_3	\	\	\	\	\	\	11.2	2.1	**9.2**	3.0	0.7	**2.3**
B_4	\	\	\	\	\	\	\	\	\	13.2	0.7	**12.5**
D_1	23.9	9.1	**14.8**	22.6	3.7	**18.9**	23.3	6.4	**29.7**	25.5	15.5	**10.0**
D_2	32.5	24.9	**7.6**	31.6	28.0	**3.5**	33.9	27.0	**6.9**	35.5	26.8	**8.7**
D_3	32.1	24.5	**7.6**	30.6	28	**2.6**	33.9	27.1	**6.8**	35.6	26.0	**9.6**

Table S5. Calculated vertical excitation energy (ΔE_{vert}) (eV), f, transition orbitals assignments, λ_{total} (eV) and k_r (s^{-1}) of designed molecules.

	ΔE_{vert}	f	assignments	λ_{total}	k_r ($\times 10^8$)
o-TSSI	1.83	1.5228	HOMO→LUMO (87.72%) HOMO-1→LUMO (9.37%)	0.4	1.5
m-TSSI	1.72	1.4400	HOMO→LUMO (84.46%) HOMO-1→LUMO (12.90%)	1.0	0.8
TSSSI	1.39	2.0423	HOMO→LUMO (80.71%) HOMO-1→LUMO (16.05%)	1.0	0.9
TSSSI	1.35	2.3405	HOMO→LUMO (74.39%) HOMO-1→LUMO (21.11%)	0.8	1.2

Table S6. The key dihedral angles (degree) for TSSI in aggregates at the S_0 and S_1 minimum.

	Agg-1			**Agg-2**			**Agg-3**		
	S_0	**S_1**	**$\|\Delta(S_0\text{-}S_1)\|$**	**S_0**	**S_1**	**$\|\Delta(S_0\text{-}S_1)\|$**	**S_0**	**S_1**	**$\|\Delta(S_0\text{-}S_1)\|$**
A_1	9.9	10.2	**0.3**	14.0	14.2	**0.2**	14.0	14.5	**0.5**
A_2	19.1	14.7	**4.4**	25.0	21.4	**3.6**	28.4	24.9	**3.5**
A_3	30.4	26.2	**4.2**	32.7	27.9	**4.8**	33.8	29.3	**4.5**
A_4	19.2	19.8	**0.6**	20.2	19.1	**1.1**	14.3	13.8	**0.5**
A_5	20.6	18.8	**4.9**	25.1	31.5	**6.4**	17.6	24.9	**7.3**
B_1	20.6	18.8	**1.8**	14.3	9.3	**5.0**	-4.1	0.4	**4.5**
B_2	32.5	37.8	**5.3**	20.8	24.7	**3.9**	17.4	23.5	**6.1**
D_1	17.0	18.8	**1.8**	29.6	35.5	**5.9**	18.2	20.5	**2.3**
D_2	52.8	54.7	**1.9**	43.0	51.7	**8.7**	44.2	55.5	**11.3**
D_3	42.7	49.6	**6.9**	43.0	53.1	**10.1**	54.5	60.4	**5.9**

Table S7. Calculated vertical excitation energy (ΔE_{vert}) (eV), f, transition orbitals assignments, λ_{total} (eV), k_r (s^{-1}) k_{ic} (s^{-1}) and Φ_F of TSSI in monomer and aggregates.

	ΔE_{vert}	f	assignments	λ_{total}	k_r ($\times 10^7$)	k_{ic} ($\times 10^6$)	Φ_F (%)
Agg-1	1.51	0.3367	HOMO→LUMO (97.76%)	0.4	2.9	6.6	81.5
Agg-2	1.47	0.2550	HOMO→LUMO (98.41%)	0.5	2.3	8.4	73.2
Agg-3	1.53	0.3493	HOMO→LUMO (97.94%)	0.3	3.0	20.7	59.2

Supplementary References

1. J. Tomasi, B. Mennucci and R. Cammi, Quantum Mechanical Continuum Solvation Models, *Chem. Rev.*, 2005, **105**, 2999-3093.
2. S. Chibani, A. Charaf-Eddin, B. L. Guennic and D. Jacquemin, Boranil and Related NBO Dyes: Insights From Theory, *J. Chem. Theory. Comput.*, 2013, **9**, 3127-3135.
3. H. B. S. G. W. T. M. J. Frisch, G. E. Scuseria, M. A. Robb, J. R. Cheeseman, G. Scalmani, V. Barone, G. A. Petersson, H. Nakatsuji, X. Li, M. Caricato, A. V. Marenich, J. Bloino, B. G. Janesko, R. Gomperts, B. Mennucci, H. P. Hratchian, J. V. Ortiz, A. F. Izmaylov, J. L. Sonnenberg, D. Williams-Young, F. Ding, F. Lipparini, F. Egidi, J. Goings, B. Peng, A. Petrone, T. Henderson, D. Ranasinghe, V. G. Zakrzewski, J. Gao, N. Rega, G. Zheng, W. Liang, M. Hada, M. Ehara, K. Toyota, R. Fukuda, J. Hasegawa, M. Ishida, T. Nakajima, Y. Honda, O. Kitao, H. Nakai, T. Vreven, K. Throssell, J. A. Montgomery, Jr., J. E. Peralta, F. Ogliaro, M. J. Bearpark, J. J. Heyd, E. N. Brothers, K. N. Kudin, V. N. Staroverov, T. A. Keith, R. Kobayashi, J. Normand, K. Raghavachari, A. P. Rendell, J. C. Burant, S. S. Iyengar, J. Tomasi, M. Cossi, J. M. Millam, M. Klene, C. Adamo, R. Cammi, J. W. Ochterski, R. L. Martin, K. Morokuma, O. Farkas, J. B. Foresman, and D. J. Fox., Gaussian16 Revision A.03. Gaussian Inc. Wallingford CT, 2016.
4. S. Grimme, J. Antony, S. Ehrlich and H. Krieg, A Consistent and Accurate ab initio Parametrization of Density Functional Dispersion Correction (DFT-D) for the 94 Elements H-Pu, *J. Chem. Phys.*, 2010, **132**, 154104.
5. Y. Tawada, T. Tsuneda, S. Yanagisawa, T. Yanai and K. Hirao, A Long-Range-Corrected Time-Dependent Density Functional Theory, *J. Chem. Phys.*, 2004, **120**, 8425-8433.
6. J. D. Chai and M. Head-Gordon, Long-Range Corrected Hybrid Density Functionals with Damped Atom-Atom Dispersion Corrections, *Phys. Chem. Chem. Phys.*, 2008, **10**, 6615-6620.
7. A. D. Boese and J. M. Martin, Development of Density Functionals for Thermochemical Kinetics, *J. Chem. Phys.*, 2004, **121**, 3405-3416.
8. Y. Zhao and D. G. Truhlar, The M06 Suite of Density Functionals for Main Group Thermochemistry, Thermochemical Kinetics, Noncovalent Interactions, Excited States, and Transition Elements: Two New Functionals and Systematic Testing of Four M06-Class Functionals and 12 Other Functionals, *Theo. Chem. Accounts.*, 2007, **120**, 215-241.
9. R. Ditchfield, W. J. Hehre and J. A. Pople, Self-Consistent Molecular-Orbital Methods. IX. An Extended Gaussian-Type Basis for Molecular-Orbital Studies of Organic Molecules, *J. Chem. Phys.*, 1971, **54**, 724-728.
10. Z. Zhang, W. Xu, M. Kang, H. Wen, H. Guo, P. Zhang, L. Xi, K. Li, L. Wang, D. Wang and B. Z. Tang, An All-Round Athlete on the Track of Phototheranostics: Subtly Regulating the Balance between Radiative and Nonradiative Decays for Multimodal Imaging-Guided Synergistic Therapy, *Adv. Mater.*, 2020, **32**, 2003210.
11. J. Wang, R. M. Wolf, J. W. Caldwell, P. A. Kollman and D. A. Case, Development and Testing of A General Amber Force Field, *J. Comput. Chem.*, 2004, **25**, 1157-1174.
12. H. J. C. Berendsen, J. P. M. Postma, W. F. van Gunsteren, A. DiNola and J. R. Haak, Molecular Dynamics with Coupling to An External Bath, *J. Chem. Phys.*, 1984, **81**, 3684-3690.
13. D. Bakowies and W. Thiel. Hybrid Models for Combined Quantum Mechanical and Molecular Mechanical Approaches, *J. Phys. Chem.*, 1996, **100**, 10580-10594.
14. D. v. d. S. M. J. Abraham, E. Lindahl and B. Hess, GROMACS User Manual version 5.1. 2015
15. A. K. Rappé, C. J. Casewit. K. S. Colwell, W. A. Goddard III and W. M. Skiff, UFF, A Full Periodic Table Force Field for Molecular Mechanics and Molecular Dynamics Simulations, *J. Am. Chem. Soc.*, 1992, **114**,

10024-10035.
16. T. Lu and F. Chen, Multiwfn: A Multifunctional Wavefunction Analyzer, *J. Comput. Chem.*, 2012, **33**, 580-592.
17. F. Neese, F. Wennmohs, U. Becker and C. Riplinger, The ORCA Quantum Chemistry Program Package, *J. Chem. Phys.*, 2020, **152**, 224108.
18. Z. Shuai, Thermal Vibration Correlation Function Formalism for Molecular Excited State Decay Rates, *Chin. J. Chem.*, 2020, **38**, 1223-1232.
19. Z. Shuai and Q. Peng, Excited States Structure and Processes: Understanding Organic Light-Emitting Diodes at the Molecular Level, *Phys. Rep.*, 2014, **537**, 123-156.
20. Y. Niu, W. Li, Q. Peng, H. Geng, Y. Yi, L. Wang, G. Nan, D. Wang and Z. Shuai, MOlecular MAterials Property Prediction Package (MOMAP) 1.0: A Software Package for Predicting the Luminescent Properties and Mobility of Organic Functional Materials, *Mol. Phys.*, 2018, **116**, 1078-1090.